

Magnetic and Thermal Properties of $\text{SmRh}_2\text{Zn}_{20}$ Single Crystal

Yosikazu Isikawa*, Toshio Mizushima, Aika Fujita, and Tomohiko Kuwai

*Graduate School of Science and Engineering, University of Toyama, Toyama 930-8555,
Japan*

The magnetization, magnetic susceptibility, and specific heat of the single crystalline sample $\text{SmRh}_2\text{Zn}_{20}$ were measured. The valence of Sm ions in $\text{SmRh}_2\text{Zn}_{20}$ was found to be trivalent. No evidence of valence fluctuations was detected. $\text{SmRh}_2\text{Zn}_{20}$ is an antiferromagnet with $T_N = 2.46$ K. The observed magnetic phase transition temperature in the $C(T, H)$ curves showed that T_N splits into two in the external field H along the [001] and [101] directions. On the other hand, T_N in H along the [111] direction did not split, decreasing to 2.20 K at $H = 7$ T. At 2 K, the magnetization M_{111} in H along the [111] direction increased linearly with increasing field, while M_{001} and M_{101} deviated upward slightly from the linear dependence. We analyzed the observed magnetic and thermal properties of $\text{SmRh}_2\text{Zn}_{20}$ taking into account the crystalline-electric-field effect, the Zeeman energy, and the exchange interaction. The theoretical calculation well reproduced the experimental $\chi(T)$, $M(H)$, $C(T, H)$ and $T_N(H)$, suggesting that the energy scheme of Sm^{3+} is composed of the ground state Γ_7 and the excited state Γ_8 with an energy gap of 10.8 K. The sublattice magnetic moments are expected to be along the $\langle 111 \rangle$ direction below T_N at $H = 0$ T. Variations of the magnetic structures induced by the external magnetic fields in a narrow temperature region around T_N are inferred on the basis of theoretical calculations.

1. Introduction

Many Sm-based compounds have been investigated for more than three decades because they show the fundamental physical properties of condensed matters such as valence fluctuation and intermediate valence.^{1,2)} Recently, RTr_2X_{20} -type compounds ($R =$ rare earth, $Tr =$ transition metal, $X =$ Al, Zn, Cd) have attracted much attention because of their various physical properties.³⁻⁸⁾ They crystallize in the cubic structure, and the rare-earth atoms are in the cubic symmetric sites. Sakai and Nakatsuji, Higashinaka et al., and Yamada et al. presented the interesting experimental results⁹⁻¹¹⁾ indicating that $\text{Sm}Tr_2\text{Al}_{20}$ ($Tr =$ Ti, V, Cr, Ta) are an-

*E-mail: isikawa@sci.u-toyama.ac.jp

tiferromagnets with strong valence fluctuation, which brought about characteristic behaviors such as a large electronic specific-heat coefficient C/T , a weak temperature dependence of magnetic susceptibility, a $-\ln T$ -dependent resistivity, and a field-insensitive phase transition. The peculiar valence fluctuation is ascribed to the strong c - f hybridization. It is contradictory, however, to the fact that the ground state of Sm ions in all $\text{SmTr}_2\text{Al}_{20}$ is said to be a quartet Γ_8 of trivalent Sm. Kuwai et al. measured¹²⁾ the thermoelectric power S of $\text{SmTr}_2\text{Al}_{20}$ ($Tr = \text{Ti, V, Cr}$) and found the large values of $\Delta S/T$ at temperatures above and near the Néel temperature T_N . The large values of S correspond approximately to the large values of C/T since S is proportional to C when both originate from the density of states of the conduction electrons at the Fermi energy.

$\text{SmTr}_2\text{Zn}_{20}$ ($Tr = \text{Fe, Co, Ru}$) and $\text{SmTr}_2\text{Cd}_{20}$ ($Tr = \text{Ni, Pd}$) have been investigated by Yazici et al.¹³⁾ and Jia et al.¹⁴⁾ $\text{SmTr}_2\text{Zn}_{20}$ ($Tr = \text{Fe, Ru}$) and $\text{SmNi}_2\text{Cd}_{20}$ exhibit ferromagnetic order, whereas $\text{SmPd}_2\text{Cd}_{20}$ is an antiferromagnet and $\text{SmCo}_2\text{Zn}_{20}$ is nonmagnetic down to 110 mK. The valence of Sm ions in these series is close to trivalent. The ground state of Sm^{3+} due to the crystalline-electric-field (CEF) effect is quartet Γ_8 for $\text{SmRu}_2\text{Zn}_{20}$ ¹⁵⁾ and $\text{SmPd}_2\text{Cd}_{20}$.¹³⁾ $\text{SmRu}_2\text{Zn}_{20}$ shows an anomalous magnetic anisotropy of magnetization below the Curie temperature T_C , which contradicts the anisotropy predicted from the Γ_8 ground state.¹⁵⁾ Isikawa et al. suggested¹⁵⁾ the possibility of the octupole-octupole interaction as a mechanism to explain the anomalous magnetic anisotropy. Yazici et al. suggested¹³⁾ that $\text{SmRu}_2\text{Zn}_{20}$ is a rare compound of Sm-based heavy-fermion ferromagnet based on the Sommerfeld–Wilson and Kadowaki–Woods ratios.

A few experimental data revealed^{16–20)} that $\text{SmIr}_2\text{Zn}_{20}$ and $\text{SmRh}_2\text{Zn}_{20}$ are antiferromagnets with T_N at 1.3 and 2.4 K, respectively. The former has an additional T_N at 1.2 K. The ground state of Sm ions is the Γ_7 doublet for both compounds, which are rare examples among the $\text{SmTr}_2\text{X}_{20}$ -type compounds. In $\text{SmRh}_2\text{Zn}_{20}$, the field-induced new phases and the field-induced first-order transition were observed. However, this first-order transition was sample-sensitive.

In this paper, we report the magnetic susceptibility $\chi(T)$, magnetization $M(H)$, and specific heat $C(T, H)$ of $\text{SmRh}_2\text{Zn}_{20}$ to elucidate the fundamental physical properties of the sample. $\text{SmRh}_2\text{Zn}_{20}$ is an antiferromagnet with a Néel temperature $T_N = 2.46$ K. The observed peak in the $C(T)$ curve at T_N is split into two by the external field H , depending on the field direction. A phase diagram of T_N vs H is given. The experimental results of $\chi(T)$, $M(H)$, $C(T, H)$, and the field-direction dependence of T_N are well reproduced by the theoretical calculations based on the CEF effect, Zeeman effect, and exchange interaction. The variations

of the magnetic structures in H are discussed on the basis of theoretical calculations.

2. Experimental Procedure

Single crystals of $\text{SmRh}_2\text{Zn}_{20}$ and the reference sample $\text{YRh}_2\text{Zn}_{20}$ were grown by the Zn-self-flux method, which was the same as that described previously.^{21,22)} The crystal structure of the cubic $\text{CeCr}_2\text{Al}_{20}$ type was confirmed from the X-ray powder diffraction pattern. There was no trace of impurity phases. The lattice parameters a of $\text{SmRh}_2\text{Zn}_{20}$ and $\text{YRh}_2\text{Zn}_{20}$ were obtained to be 14.226 and 14.200 Å, respectively, which agree with those in the literature.^{23,24)} The crystal axis was determined from Laue pictures. The samples were shaped using a spark-cutting machine, and the weights of the samples $\text{SmRh}_2\text{Zn}_{20}$ and $\text{YRh}_2\text{Zn}_{20}$ are 4.46 and 7.67 mg, respectively, which were used for all the measurements. We recognized a sample dependence of the physical properties in $\text{SmRh}_2\text{Zn}_{20}$; thus, we present here the data of the sample, the specific heat $C(T)$ of which shows the sharpest peak at T_N and the highest T_N .

The magnetization M and the magnetic susceptibility χ were measured at temperatures down to 2.0 K using a magnetic property measurement system (MPMS, Quantum Design Inc.). The specific heat was measured at temperatures down to 0.5 K using a physical property measurement system (PPMS, Quantum Design Inc.).

3. Experimental Results

Figure 1 shows the temperature dependence of the magnetic susceptibility of $\text{SmRh}_2\text{Zn}_{20}$ in the field 1 T along the [001] direction. The value of χ at 300 K suggests that the Sm ions in $\text{SmRh}_2\text{Zn}_{20}$ are in the trivalent state, not in the valence-mixing state.¹⁾ The magnetism of the trivalent Sm compound is generally expressed by the sum of two components: the Curie term that originated from $J = 5/2$ and the Van Vleck term that originated from the mixing of $J = 5/2$ with $7/2$, that is, $\chi^{3+}(T) = C/T + \chi_{\text{VV}}$, where C is the Curie constant of $J = 5/2$. In addition, the magnetic susceptibility is affected by the exchange interaction as follows: $1/\chi = 1/\chi^{3+} - n$. The solid line in Fig. 1 shows the calculated $\chi(T)$ curve using the two parameters, $\chi_{\text{VV}} = 0.97 \times 10^{-3}$ emu/mol and $n = -47$ mol/emu. The experimental susceptibility is in good agreement with the calculated one. The inset in Fig. 1 shows the reciprocal susceptibility $1/\chi$ and corrected reciprocal susceptibility $1/(\chi(T) - \chi_{\text{VV}})$ at temperatures below 30 K in the same field as in the main figure. The corrected susceptibility shows a linear dependence of temperature representing the usual Curie–Weiss law. The thick solid line in the inset is the calculated line using n . At low temperatures between 3 and 30 K, the experimental data is also in good agreement with the calculated one. The good agreement at temperatures between 3

and 300 K indicates that the CEF effect is small. The paramagnetic Curie temperature θ_p was deduced to be -5 K from the data in Fig. 1, which is related theoretically to the parameter n as $\theta_p = nC$.

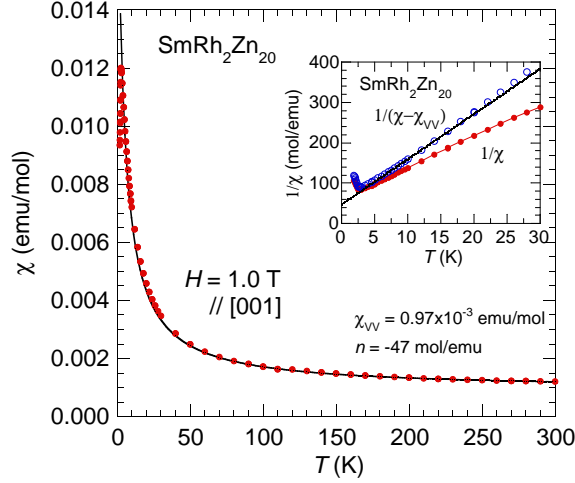


Fig. 1. (Color online) Magnetic susceptibility of $\text{SmRh}_2\text{Zn}_{20}$ in the field 1 T along the [001] direction. The solid line is a calculated curve. Inset: reciprocal magnetic susceptibilities $1/\chi$ (closed red circles) and $1/(\chi-\chi_{VV})$ (blue open circles) in low-temperature region. The thick solid line in the inset is a calculated curve. See text for details.

Figure 2 shows the $\chi(T)$ curve in the field 1 T along the [001] direction at low temperatures. The magnetic phase transition T_N is observed at 2.46 K. The temperature dependences of $\chi(T)$ along the [101] and [111] directions were also measured (not shown here) and they were almost the same as that along the [001] direction at temperatures down to 2 K, implying that $\chi(T)$ does not show any field-direction dependence even at temperatures below T_N . However, the absence of the field-direction dependence of $\chi(T)$ is limited at temperatures in the vicinity of T_N . The inset in Fig. 2 shows the field dependences of magnetization at 2 K in the fields along the [001], [101], and [111] directions. The magnetization along the [111] direction shows an almost linear dependence against the field, but the magnetizations along the [001] and [101] directions gradually deviate upward slightly from the linear dependence at around 2 T. This result does not indicate that the easy direction of magnetization in fields is parallel to the [001] or [101] direction.

Figure 3 shows the temperature dependences of the specific heat C of $\text{SmRh}_2\text{Zn}_{20}$ and $\text{YRh}_2\text{Zn}_{20}$. The sharp peak at T_N is observed at 2.46 K, which is the same temperature as that determined in the $\chi(T)$ curve. The magnetic component C_{mag} of the specific heat is evaluated

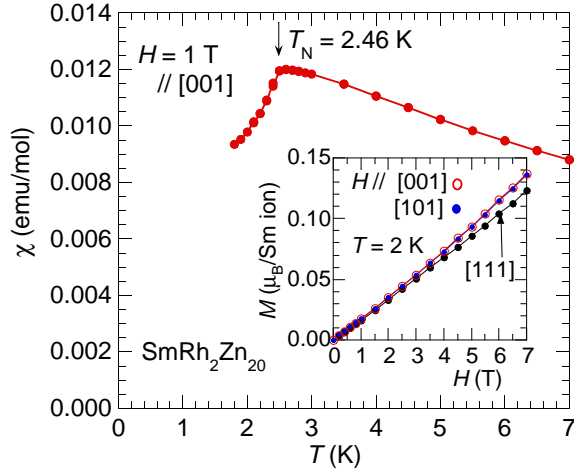


Fig. 2. (Color online) Magnetic susceptibility of $\text{SmRh}_2\text{Zn}_{20}$ in the field 1 T along the [001] direction at temperatures below 7 K. Inset: magnetization curves at 2 K in the fields along the [001], [101], and [111] directions.

as $C_{\text{SmRh}_2\text{Zn}_{20}} - C_{\text{YRh}_2\text{Zn}_{20}}$ and is shown by the black open circles in this figure. The entropy S is numerically calculated by integrating C/T on T and is shown in the inset in Fig. 3. The entropy at T_N is approximately equal to $R \ln 2$, indicating that the ground state of Sm^{3+} is doublet Γ_7 . Moreover, the rapid increase in entropy above T_N with increasing temperature suggests that the excited state Γ_8 is close to the ground state. The thick solid line indicated by C_{Schottky} in Fig. 3 shows the calculated $C(T)$ curve of $\text{SmRh}_2\text{Zn}_{20}$, where the energy scheme was assumed to be composed of the doublet ground state and the quartet excited state with a gap $\Delta = 10.8$ K. The solid line indicated by S_{Schottky} in the inset is the calculated entropy $S(T)$ curve. The calculated two lines are in good agreement with the experimental ones above T_N . This narrow energy gap indicates that the CEF effect is weak, which is consistent with the consideration of the temperature dependence of $\chi(T)$ above T_N . $\chi(T)$ was mostly understood on the basis of the Curie–Weiss law of Sm^{3+} without the CEF effect.

Figures 4(a)–4(c) show the temperature dependences of the specific heat of $\text{SmRh}_2\text{Zn}_{20}$ in magnetic fields along the [001], [101], and [111] directions. Interestingly, in the fields along the [001] and [101] directions, T_N splits into two and the width of splitting increases with increasing field. The upper T_N does not change with increasing field, whereas the lower one decreases with increasing field. In the field along the [111] direction, T_N gradually decreases without splitting. Figure 4(d) shows the field-direction dependence of T_N . The splitting widths of T_N at 7 T are 0.26 K in $H // [001]$ and 0.14 K in $H // [101]$. These of T_N changes appear in the narrow temperature range between 2.16 and 2.46 K.

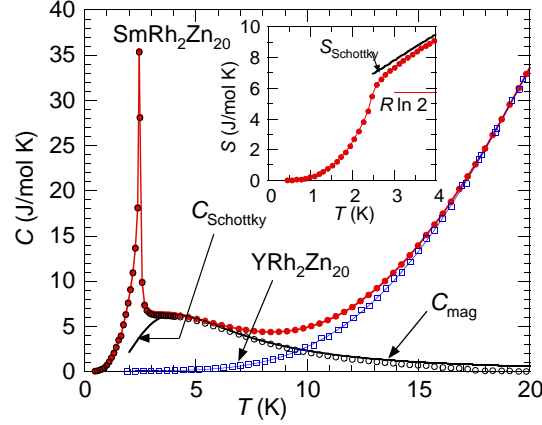


Fig. 3. (Color online) Temperature dependences of the specific heat C of $\text{SmRh}_2\text{Zn}_{20}$ (red closed circles) and $\text{YRh}_2\text{Zn}_{20}$ (blue open squares). C_{mag} denotes the magnetic part of C (black open circles) evaluated as $C_{\text{SmRh}_2\text{Zn}_{20}} - C_{\text{YRh}_2\text{Zn}_{20}}$. The thick solid line denoted by C_{Schottky} is a calculated curve of the Schottky-type specific heat. Inset: temperature dependence of the entropy of $\text{SmRh}_2\text{Zn}_{20}$. The solid line denoted by S_{Schottky} is a calculated curve. See text for details.

4. Analysis and Discussion

4.1 Hamiltonian

We discuss the small magnetic anisotropy observed in the magnetization curves at 2 K (inset in Fig. 2), the field-direction dependence of the specific heat $C(T)$, and the complex behaviors of T_N in fields (Fig. 4). Generally, as a consequence of the characteristics of Γ_7 and Γ_8 of Sm^{3+} in the cubic symmetry, the Γ_7 state is magnetically isotropic, whereas the Γ_8 state is anisotropic in fields. Thus, it is expected that this magnetic anisotropy will be caused by the mixing of the Γ_8 state with the ground state Γ_7 through the external magnetic field and the exchange field. We analyze this magnetic anisotropy in the frame of the molecular-field approximation. For simplicity, a simple antiferromagnetic structure with two sublattices (A and B) is assumed, that is, the up- and down-magnetic moments are fixed in the A and B sublattices, respectively. We define the following Hamiltonian to analyze the magnetic and thermal properties of Sm^{3+} in $\text{SmRh}_2\text{Zn}_{20}$,

$$\mathcal{H}_i = A_4(O_4^0 + 5 O_4^4) + g_J \mu_B \mathbf{J}_i \mathbf{H}_{\text{ext}} + g_J \mu_B \mathbf{J}_i \mathbf{H}_{\text{mol}}(i), \quad (1)$$

where i denotes the sublattices (A and B). The first term in this equation is the CEF energy,^{25–27)} where the six-order term in the CEF energy is excluded because the quantum number J is $5/2$. The mixing effect with the upper multiplet of $J = 7/2$ will be taken into account by adding χ_{VV} to χ calculated using Eq. (1). The second term in Eq. (1) is the Zeeman energy due to the external magnetic field \mathbf{H}_{ext} , and the third term is the exchange energy expressed in

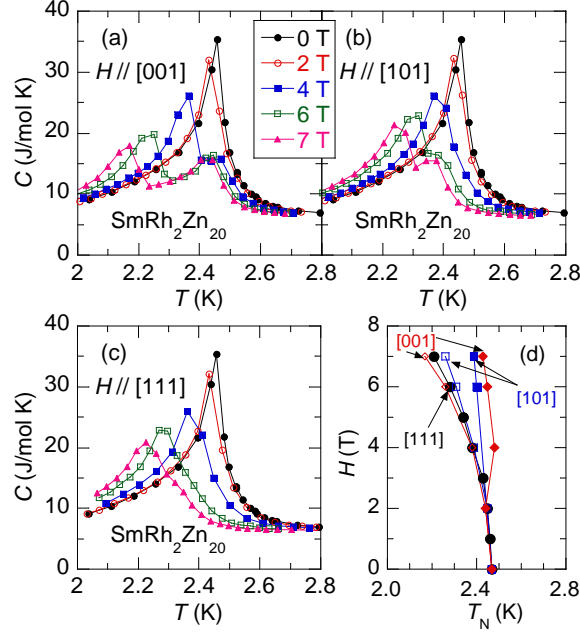


Fig. 4. (Color online) Temperature dependences of the specific heat C of $\text{SmRh}_2\text{Zn}_{20}$ in magnetic fields along the [001] (a), [101] (b), and [111] (c) directions. (d) Magnetic field dependences of T_N in the fields along the [001] (filled and open diamonds), [101] (filled and open squares), and [111] (filled circles) directions. See text for details.

the molecular-field approximation. The molecular field $\mathbf{H}_{\text{mol}}(i)$ at the i sublattice is expressed using the average magnetic moment in the other sublattice j as $n_{\text{BA}}(g_J\mu_B)\langle\mathbf{J}_j\rangle$, where $\langle\cdots\rangle$ is the thermal average and n_{BA} is the exchange coupling parameter between the atoms in the A and B sublattices. The other parameters used in Eq. (1) are conventionally defined.^{25,26)}

The average magnetization at each sublattice is calculated as

$$\mathbf{M}_i = -g_J\mu_B\langle\mathbf{J}_i\rangle = -g_J\mu_B\frac{\text{Tr } \mathbf{J}_i \exp(-\beta\mathcal{H}_i)}{\text{Tr } \exp(-\beta\mathcal{H}_i)}, \quad (2)$$

where $\beta = 1/k_B T$. The average magnetization \mathbf{M} per atom is $\mathbf{M} = (\mathbf{M}_A + \mathbf{M}_B)/2$. Note that the physical quantities of \mathbf{J}_i , \mathbf{H}_{mol} , and \mathbf{H}_{ext} are three-dimensional vectors. Thus, Eq. (2) is a set of six equations, which represent the thermal averages of the x -, y -, and z -components of \mathbf{M}_A and \mathbf{M}_B . Equation (2) is solved by the iteration method. By using both values of $\langle\mathbf{J}_A\rangle$ and $\langle\mathbf{J}_B\rangle$, which have been obtained using Eq. (2), the specific heat C per mole is evaluated as

$$C = \left(\frac{N_A}{2}\right) \frac{\partial}{\partial T} \left(\langle\mathcal{H}_A\rangle + \langle\mathcal{H}_B\rangle - \frac{1}{2}\langle\mathcal{H}_{\text{exch}}\rangle \right), \quad (3)$$

where N_A is Avogadro's number, and the third term in parentheses is used to correct the double counting of the exchange energy between the Sm atoms at A and B sublattices. $\mathcal{H}_{\text{exch}}$

in this equation is the same as the third term in Eq. (1) and is expressed as $n_{\text{BA}}(g_J\mu_{\text{B}})^2\mathbf{J}_{\text{A}}\mathbf{J}_{\text{B}}$.

We have only two fitting parameters, i.e., A_4 and n_{BA} , when we numerically calculate $M(T, H)$ and $C(T, H)$ using the above Hamiltonians, where H is the magnitude of \mathbf{H}_{ext} . A_4 is proportional to Δ as $A_4 = \Delta/360$ in the unit [K], and n_{BA} is physically the same as n [mol/emu] through the relationship of $n_{\text{BA}} = nN_{\text{A}}$. As already mentioned in Sect. 3, the energy scheme of Sm^{3+} is composed of the doublet ground state Γ_7 and the quartet excited state Γ_8 with $\Delta = 10.8$ K. Thus, A_4 is set to be 0.030 [K]. The value of n_{BA} was accurately determined to be $-1.45 k_{\text{B}}/(g_J\mu_{\text{B}})^2$ by adjusting the calculated T_{N} to the experimental T_{N} . Consequently, the sublattice magnetic moments M_{A} and M_{B} are evaluated as a result of the iteration process of Eq. (2) using the two parameters A_4 and n_{BA} . This means that the magnetic alignments of each sublattice moment in H are inferred. First, we present the calculated results of $\chi(T)$, $M(H)$, $C(T, H)$, and $T_{\text{N}}(H)$ in comparison with the respective experimental data in the next subsection. After that, we discuss the magnetic alignments of sublattice magnetic moments in H .

We have to note one important result concluded from this CEF calculation. At temperatures below T_{N} , the magnetic moments at the sublattices are along the $\langle 111 \rangle$ direction at $H = 0$, namely, there exist four magnetic domains below T_{N} . For simplicity, we have calculated the $\chi(T)$, $M(H)$, and $C(T)$ curves in fields for a single domain, in which the up- and down-magnetic moments are along the $[111]$ and $[\bar{1}\bar{1}\bar{1}]$ directions, respectively.

4.2 Calculation and comparison with the experimental data

Figure 5 shows the calculated temperature dependences of the magnetic susceptibility χ of $\text{SmRh}_2\text{Zn}_{20}$ in the field 1 T along the $[001]$, $[101]$, and $[111]$ directions, where χ has been shifted by the amount of χ_{VV} because the mixing effect with the multiplet of $J = 7/2$ is not taken into account in Eq. (2). In the temperature range between 2 K and T_{N} , the magnetic anisotropy is very small, which is consistent with the experimental results. Below 2 K, however, the calculated χ shows a magnetic anisotropy, although we cannot compare it with the experimental data, which is limited above 2 K.

The inset in Fig. 5 shows the calculated magnetization curves at 2 K in the fields along the $[001]$, $[101]$, and $[111]$ directions. $M_{111}(H)$ in $H // [111]$ increases linearly with increasing field without any anomalies such as spin flops, which is in good agreement with the experimental behavior. On the other hand, the $M_{101}(H)$ curve deviates slightly from the $M_{111}(H)$ curve around 3 T, and the $M_{001}(H)$ curve deviates further from the $M_{111}(H)$ curve. The characteristic behaviors of the three calculated $M(H)$ curves at 2 K are in good agreement with

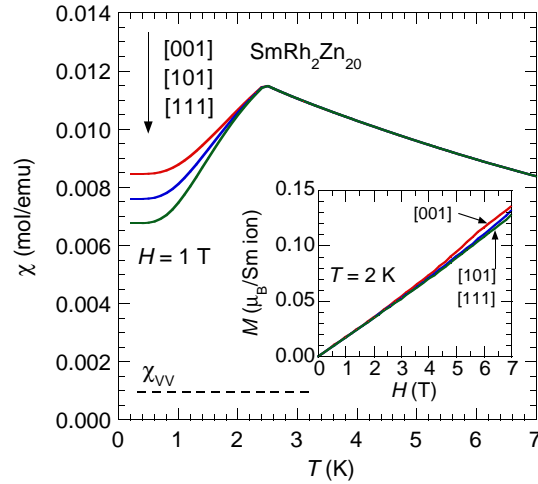


Fig. 5. (Color online) Temperature dependences of the calculated magnetic susceptibility of $\text{SmRh}_2\text{Zn}_{20}$ in the field 1 T along the [001], [101], and [111] directions. Inset: calculated magnetization curves at 2 K along the three directions. See text for details.

the experimental ones.

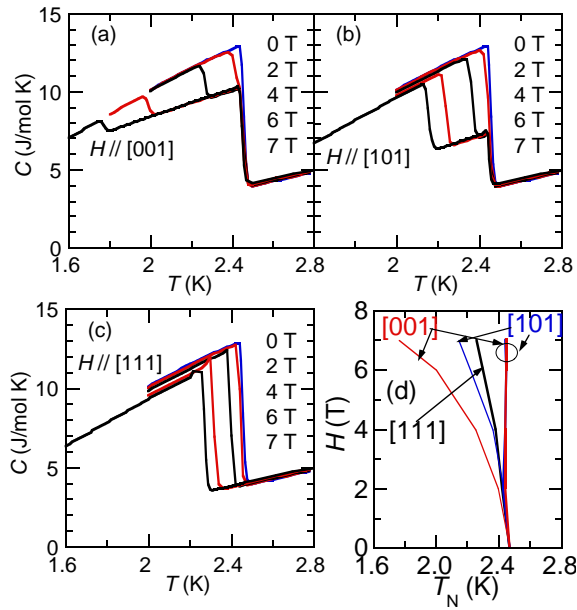


Fig. 6. (Color online) Temperature dependences of the calculated specific heat of $\text{SmRh}_2\text{Zn}_{20}$ in the fields along the [001] (a), [101] (b), and [111] (c) directions. (d) Calculated field dependences of T_N . See text for details.

Figures 6(a)–6(c) show the calculated specific heat C in the fields of 0, 2, 4, 6, and 7 T along the [001], [101], and [111] directions. In the case of $H // [001]$ and [101], T_N splits into two, and the width of the splitting increases with increasing field. In $H // [111]$, T_N does not

split but moderately decreases with increasing H . In Fig. 6(d), the external-field dependences of T_N are plotted. The splitting widths of T_N at 7 T are 0.7 K in $H // [001]$, 0.3 K in $H // [101]$, and zero in $H // [111]$. These characteristic behaviors are also in good agreement with the experimental ones. However, note that the height of the calculated specific heat at T_N at 0 T is one-third compared with that of the experimental specific heat at T_N , and the second-peak height separated by H is also lowered compared with the experimental one. This is caused by the fact that the numerical calculation is based on the molecular-field approximation. The magnetic fluctuation $\langle(\mathbf{J}_A - \langle\mathbf{J}_A\rangle)(\mathbf{J}_B - \langle\mathbf{J}_B\rangle)\rangle$, which is more important in the vicinity of T_N than at temperatures far from T_N , cannot be taken into account in this approximation. In fact, at 2.0 and 2.8 K, which are far below and far above T_N , respectively, the values of the calculated C are approximately equal to those of the experimental C .

It is concluded that the theoretical calculations have successfully reproduced the macroscopic experimental data, $\chi(T)$, $M(T, H)$, $C(T, H)$, and $T_N(H)$, by using only two parameters, A_4 and n_{BA} .

4.3 Alignment of sublattice magnetic moments

In this subsection, we present the microscopic magnetic structures of $\text{SmRh}_2\text{Zn}_{20}$ in the vicinity of T_N , which have been deduced from the model calculations. Here, we discuss the single magnetic domain.

Figures 7(a)–7(c) show the temperature dependences of the calculated x -, y -, and z -components of the respective sublattice magnetic moments of $\text{SmRh}_2\text{Zn}_{20}$ in the field 4 T. The subscripts 1 and 2 denote the up- and down-sublattice moments, respectively. In H along the $[001]$ direction, as seen in Fig. 7(a), the lower T_N is found to be the temperature at which the antiferromagnetic alignment along the $[001]$ direction (z -component) disappears, and the upper T_N is the temperature at which the antiferromagnetic alignment of both the x - and y -components disappears. In H along the $[101]$ direction [Fig. 7(b)], the lower T_N is the temperature at which the antiferromagnetic alignment along the $[101]$ direction disappears, and the upper T_N is the temperature at which the antiferromagnetic alignment of the y -component disappears. In H along the $[111]$ direction [Fig. 7(c)], the magnetizations \mathbf{M}_A and \mathbf{M}_B are parallel to the $[111]$ direction, and the antiferromagnetic alignment disappears at T_N . Thus, the magnetic susceptibility along the $[111]$ direction can be considered a parallel magnetic susceptibility. In the cases of H along the $[001]$ and $[101]$ directions, the antiferromagnetic component along the H directions disappears at temperatures between the lower and upper T_N 's. Thus, the magnetic susceptibility along these directions can be considered a perpen-

dicular magnetic susceptibility. The lower and upper T_N 's as well as the T_N along the [111] direction are second-order phase-transition temperatures.

Figures 8(a)–8(c) show the field dependences of the calculated x -, y -, and z -components of the respective sublattice magnetic moments of $\text{SmRh}_2\text{Zn}_{20}$ at 2.3 K. In the cases of H along the [001] and [101] directions, as seen in Figs. 8(a) and 8(b), the antiferromagnetic alignments along the H directions disappear near 4 and 5 T, respectively. At these points, any anomalous discontinuity such as spin flopping is not theoretically concluded. On the other hand, the antiferromagnetic alignments perpendicular to the H directions are robust against H as seen in the figures. In H along the [111] direction [Fig. 8(c)], the magnetic moments \mathbf{M}_A and \mathbf{M}_B are parallel to the H direction below 6 T. Thus, the magnetization along this direction is due to the parallel susceptibility, as mentioned previously.

The susceptibility χ_{111} in H along the [111] direction has been considered the parallel susceptibility $\chi_{//}$. However, as seen in Fig. 5, the calculated $\chi_{111}(T)$ does not approach zero at 0 K. This behavior is contrary to the common behaviors of usual antiferromagnets. We briefly comment on the discrepancy between the calculated $\chi_{//}(T)$ and the $\chi(T)$ for usual antiferromagnets, although the experimental $\chi(T)$ is limited above 2 K. In the case of usual antiferromagnets, the sublattice moments \mathbf{M}_A and \mathbf{M}_B are saturated at 0 K, and they do not change even if H is applied; thus, $\chi_{//}$ is equal to zero. However, when $\Delta \neq 0$, the sublattice moments \mathbf{M}_A and \mathbf{M}_B are not saturated at 0 K, that is, the moment \mathbf{M}_A increases and \mathbf{M}_B decreases with the application of the external field via a Van Vleck-type mechanism between Γ_7 and Γ_8 states in Sm^{3+} ; thus, $\chi_{//}$ is not equal to zero.

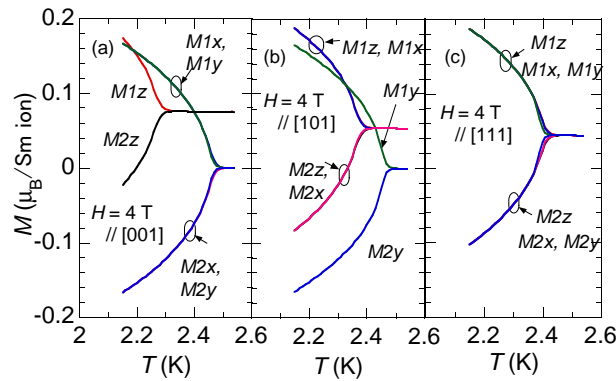


Fig. 7. (Color online) Temperature dependences of the calculated x -, y -, and z -components of respective sublattice magnetic moments of $\text{SmRh}_2\text{Zn}_{20}$ in the field 4 T along the [001] (a), [101] (b), and [111] (c) directions. The subscripts 1 and 2 denote the up- and down-sublattice moments, respectively.

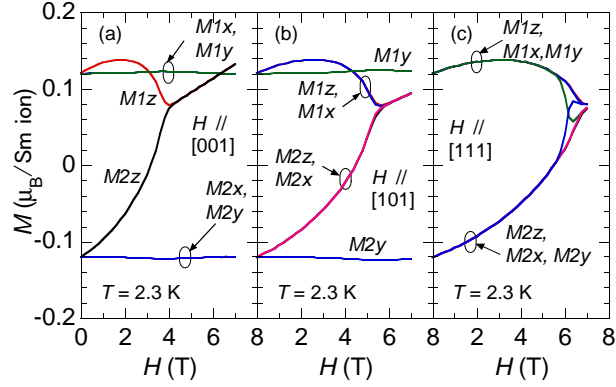


Fig. 8. (Color online) Field dependences of the calculated x -, y -, and z -components of respective sublattice magnetic moments of $\text{SmRh}_2\text{Zn}_{20}$ at 2.3 K in fields along the [001] (a), [101] (b), and [111] (c) directions. The subscripts 1 and 2 denote the up- and down-sublattice moments, respectively.

The microscopic magnetic structures deduced from the theoretical calculations have provided an insight into $\text{SmRh}_2\text{Zn}_{20}$. To confirm the magnetic structures of $\text{SmRh}_2\text{Zn}_{20}$, neutron scattering experiments should be performed.

4.4 Conclusions

We prepared single crystals of $\text{SmRh}_2\text{Zn}_{20}$ and measured $\chi(T)$, $M(T, H)$, and $C(T, H)$. Sm ions in $\text{SmRh}_2\text{Zn}_{20}$ are in the trivalent state, not in the valence fluctuating state. $\text{SmRh}_2\text{Zn}_{20}$ is an antiferromagnet with $T_N = 2.46$ K. T_N splits into two in $H \parallel [001]$ and [101]. The upper T_N does not change in fields up to the maximum H of 7 T, whereas the lower T_N decreases. In $H \parallel [111]$, T_N does not split and decreases to 2.20 K at 7 T. At 2 K, the magnetization M_{111} along the [111] direction increases linearly with increasing field, whereas M_{001} and M_{101} deviate upward slightly from the linear dependence of M_{111} . We analyzed these magnetic and thermal properties of $\text{SmRh}_2\text{Zn}_{20}$ taking into account the CEF effect, Zeeman energy, and exchange interaction. The theoretical calculations have successfully reproduced the experimental $\chi(T)$, $M(H)$, $C(T, H)$, and $T_N(H)$. The energy scheme of Sm^{3+} obtained is composed of the ground state Γ_7 and the excited state Γ_8 with the energy gap of 10.8 K. The sublattice magnetic moments are along the $\langle 111 \rangle$ direction below T_N at $H = 0$ T. The magnetic structures in magnetic fields in the temperature region between the split T_N 's could be inferred on the basis of the theoretical calculations.

Acknowledgment

We would like to thank K. Nishimura for the critical reading of our manuscript and many useful discussions.

References

- 1) J. M. Tarascon, Y. Isikawa, B. Chevalier, J. Etourneau, P. Hagenmuller, and M. Kasaya, *J. Phys. (Paris)* **41**, 1135 (1980).
- 2) J. M. Tarascon, Y. Isikawa, B. Chevalier, J. Etourneau, P. Hagenmuller, and M. Kasaya, *J. Phys. (Paris)* **41**, 1141 (1980).
- 3) T. Onimaru, K. T. Matsumoto, Y. F. Inoue, K. Umeo, Y. Saiga, Y. Matsushita, R. Tamura, K. Nishimoto, I. Ishii, T. Suzuki, and T. Takabatake, *J. Phys. Soc. Jpn.* **79**, 033704 (2010).
- 4) N. Nagasawa, T. Onimaru, K. T. Matsumoto, K. Umeo, and T. Takabatake, *J. Phys.: Conf. Ser.* **391**, 012051 (2012).
- 5) T. Onimaru, N. Nagasawa, K. T. Matsumoto, K. Wakiya, K. Umeo, S. Kittaka, T. Sakakibara, Y. Matsushita, and T. Takabatake, *Phys. Rev. B* **86**, 184426 (2012).
- 6) M. S. Torikachvili, S. Jia, E. D. Mun, S. T. Hannahs, R. C. Black, W. K. Neils, D. Martien, S. L. Bud'ko, and P. C. Canfield, *Proc. Natl. Acad. Sci. U.S.A.* **104**, 9960 (2007).
- 7) Y. Isikawa, T. Mizushima, S. Miyamoto, K. Kumagai, M. Nakahara, H. Okuyama, T. Tayama, and T. Kuwai, *J. Korean Phys. Soc.* **63**, 644 (2013).
- 8) Y. Isikawa, J. Ejiri, T. Mizushima, and T. Kuwai, *J. Phys. Soc. Jpn.* **82**, 123708 (2013).
- 9) A. Sakai and S. Nakatsuji, *Phys. Rev. B* **84**, 201106(R) (2011).
- 10) R. Higashinaka, T. Maruyama, A. Nakama, R. Miyazawa, Y. Aoki, and H. Sato, *J. Phys. Soc. Jpn.* **80**, 093703 (2011).
- 11) A. Yamada, R. Higashinaka, R. Miyazaki, K. Fushiya, T. D. Matsuda, Y. Aoki, W. Fujita, H. Harima, and H. Sato, *J. Phys. Soc. Jpn.* **82**, 123710 (2013).
- 12) T. Kuwai, T. Furuyama, K. Tada, T. Mizushima, and Y. Isikawa, *J. Phys. Soc. Conf. Proc.* **3**, 011040 (2014).
- 13) D. Yazici, B. D. White, P.-C. Ho, N. Kanchanavatee, K. Huang, A. J. Friedman, A. S. Wong, V. W. Burnett, N. R. Dilley, and M. B. Maple, *Phys. Rev. B* **90**, 144406 (2014).
- 14) S. Jia, N. Ni, S. L. Bud'ko, and P. C. Canfield, *Phys. Rev. B* **80**, 104403 (2009).
- 15) Y. Isikawa, T. Mizushima, J. Ejiri, and T. Kuwai, *J. Phys. Soc. Jpn.* **83**, 073701 (2014).
- 16) Y. Taga, K. Sugiyama, K. Enoki, Y. Hirose, K. Iwakawa, A. Mori, K. Ishida, T. Takeuchi, M. Hagiwara, K. Kindo, R. Settai, and Y. Onuku, *J. Phys. Soc. Jpn.* **81**, SB051 (2012).
- 17) M. Tanahashi, K. Adachi, T. Sasahara, N. Kase, T. Nakano, and N. Takeda, *Abstr. Meet. Physical Society of Japan (2015 Autumn Meet.)*, Part 3, p. 1858, 17aPS64 [in Japanese].

- 18) M. Tanahashi, K. Adachi, T. Sasahara, N. Kase, T. Nakano, N. Takeda, Y. Kono, and T. Sakakibara, Abstr. Meet. Physical Society of Japan (2015 Annual Meet.), Part 3, p. 2184, 22aPS94 [in Japanese].
- 19) K. Adachi, T. Sasahara, N. Kase, T. Nakano, and N. Takeda, Abstr. Meet. Physical Society of Japan (2014 Annual Meet.), Part 3, p. 623, 28aPS132 [in Japanese].
- 20) T. Sasahara, T. Nakano, and N. Takeda, Abstr. Meet. Physical Society of Japan (2013 Annual Meet.), Part 3, p. 626, 27aPS69 [in Japanese].
- 21) Y. Isikawa, T. Mizushima, K. Kumagai, and T. Kuwai, J. Phys. Soc. Jpn. **82**, 083711 (2013).
- 22) Y. Isikawa, T. Mizushima, J. Ejiri, S. Kitayama, K. Kumagai, T. Kuwai, P. Bordet, and P. Lejay, J. Phys. Soc. Jpn. **84**, 074707 (2015).
- 23) T. Nasch, W. Jeitschko, and U. C. Rodewald, Z. Naturforsch. B **52**, 1023 (1997).
- 24) S. Jia, N. Ni, G. D. Samolyuk, A. Kracher, K. Dennis, H. Ko, G. J. Miller, S. L. Bud'ko, and P. C. Canfield, Phys. Rev. B **77**, 104408 (2008).
- 25) M. T. Hutchings, Solid State Phys. **16**, 227 (1964).
- 26) K. R. Lea, M. J. M. Leask, and W. P. Wolf, J. Phys. Chem. Solids, **23**, 1381 (1962).
- 27) In the notation of Lea et al.,²⁶⁾ A_4 is equal to $Wx/60$.